JGR Atmospheres

RESEARCH ARTICLE
10.1029/2023JD039480

Key Points:

- Large-scale stratospheric cooling and circulation changes are observed following the Hunga Tonga-Hunga Ha'apai eruption
- Observations show ozone reduction in the Southern Hemisphere wintertime midlatitudes and large springtime Antarctic ozone losses in 2022
- A chemistry-climate model can track the plumes and capture observed responses to the volcanic eruption

Supporting Information:

Supporting Information may be found in the online version of this article.

Correspondence to:

X. Wang,
xinyuew@colorado.edu

Citation:

Wang, X., Randel, W., Zhu, Y., Tilmes, S., Starr, J., Yu, W., et al. (2023). Stratospheric climate anomalies and ozone loss caused by the Hunga Tonga-Hunga Ha'apai volcanic eruption. *Journal of Geophysical Research: Atmospheres*, *128*, e2023JD039480. https://doi.org/10.1029/2023JD039480

Received 22 JUN 2023
Accepted 1 NOV 2023

Author Contributions:

Conceptualization: William Randel, Yunqian Zhu, Simone Tilmes, Owen B. Toon
Data curation: William Randel, Yunqian Zhu, Simone Tilmes, Jon Starr, Wandi Yu, Adam Bourassa, Landon Rieger, Taran Warnock
Formal analysis: William Randel, Yunqian Zhu, Simone Tilmes, Jon Starr, Wandi Yu
Investigation: William Randel, Yunqian Zhu, Simone Tilmes, Rolando Garcia, Owen B. Toon, Mijeong Park, Douglas Kinnison, Jun Zhang, Adam Bourassa, Landon Rieger, Jianghanyang Li
Methodology: William Randel, Yunqian Zhu, Simone Tilmes, Wandi Yu, Rolando Garcia, Owen B. Toon, Mijeong Park, Douglas Kinnison, Adam Bourassa, Landon Rieger, Taran Warnock

Stratospheric Climate Anomalies and Ozone Loss Caused by the Hunga Tonga-Hunga Ha'apai Volcanic Eruption

Xinyue Wang[1,2], William Randel[2], Yunqian Zhu[3,4,5], Simone Tilmes[2], Jon Starr[2], Wandi Yu[6,7], Rolando Garcia[2], Owen B. Toon[1,4], Mijeong Park[2], Douglas Kinnison[2], Jun Zhang[2], Adam Bourassa[8], Landon Rieger[8], Taran Warnock[8], and Jianghanyang Li[3,9]

[1]Department of Atmospheric and Oceanic Sciences, University of Colorado Boulder, Boulder, CO, USA, [2]Atmospheric Chemistry Observations & Modeling Laboratory, National Center for Atmospheric Research, Boulder, CO, USA, [3]Cooperative Institute for Research in Environmental Sciences, University of Colorado Boulder, Boulder, CO, USA, [4]Laboratory for Atmospheric and Space Physics, University of Colorado Boulder, Boulder, CO, USA, [5]Chemical Sciences Laboratory, National Oceanic and Atmospheric Administration, Boulder, CO, USA, [6]Department of Atmospheric and Planetary Sciences, Hampton University, Hampton, VA, USA, [7]Lawrence Livermore National Laboratory, Livermore, CA, USA, [8]Institute of Space and Atmospheric Studies, University of Saskatchewan, Saskatoon, SK, Canada, [9]Institute of Arctic and Alpine Research, University of Colorado Boulder, Boulder, CO, USA

Abstract The Hunga Tonga-Hunga Ha'apai (HTHH) volcanic eruption in January 2022 injected unprecedented amounts of water vapor (H_2O) and a moderate amount of the aerosol precursor sulfur dioxide (SO_2) into the Southern Hemisphere (SH) tropical stratosphere. The H_2O and aerosol perturbations have persisted during 2022 and early 2023 and dispersed throughout the atmosphere. Observations show large-scale SH stratospheric cooling, equatorward shift of the Antarctic polar vortex and slowing of the Brewer-Dobson circulation. Satellite observations show substantial ozone reductions over SH winter midlatitudes that coincide with the largest circulation anomalies. Chemistry-climate model simulations forced by realistic HTHH inputs of H_2O and SO_2 qualitatively reproduce the observed evolution of the H_2O and aerosol plumes over the first year, and the model exhibits stratospheric cooling, circulation changes and ozone effects similar to observed behavior. The agreement demonstrates that the observed stratospheric changes are caused by the HTHH volcanic influences.

Plain Language Summary The Hunga Tonga-Hunga Ha'apai (HTHH) submarine volcano (21°S, 175°W) eruption in January 2022 injected unprecedented amounts of water vapor (H_2O) as well as moderate amounts of aerosol precursor sulfur dioxide (SO_2) into the stratosphere. The H_2O and aerosol perturbations persisted throughout 2022 and were accompanied by large changes in stratospheric climate and ozone chemistry. We use a chemistry-climate model forced by realistic HTHH inputs of H_2O and SO_2 to simulate these stratospheric changes. The model exhibits temperature, circulation, and ozone anomalies in response to these forcings that are similar to those observed. The agreement demonstrates that the observed anomalies impacts are caused by HTHH volcanic influences.

1. Introduction

Global ozone levels are recovering due to reductions of CFCs in the stratosphere as the result of the Montreal Protocol and its amendments. However, natural impacts from wildfires (Santee et al., 2022; Solomon et al., 2022, 2023; Strahan et al., 2022) or from large volcanic eruptions (Stone et al., 2017) can temporarily impact stratospheric ozone. The Hunga Tonga-Hunga Ha'apai (HTHH) submarine volcano erupted on 15 January 2022 and increased the global stratospheric water burden by ∼10%, setting a record for the modern satellite era and differentiating itself from previous major volcanic eruptions (Khaykin et al., 2022; Millan et al., 2022; Randel et al., 2023; Vömel et al., 2022). The excess moisture is expected to remain in the stratosphere for several years and could exert a substantial impact on the climate system (Jenkins et al., 2023; Li & Newman, 2020; Solomon et al., 2010). A moderate amount of sulfur-containing gases, approximately 0.4–0.5 Tg sulfur dioxide (SO_2), about 30 times lower than the emission from Pinatubo (Carn et al., 2022), was lofted into the stratosphere by the HTHH eruption and quickly converted to sulfate aerosol particles (Zhu et al., 2022). Simulations carried out with the Whole Atmosphere Community Climate Model (WACCM), a coupled chemistry-climate model, suggest the excessive moisture halves the SO_2 lifetime and promotes faster sulfate aerosol formation, resulting in large perturbations to

Resources: William Randel, Yunqian Zhu, Simone Tilmes
Software: Yunqian Zhu, Simone Tilmes, Wandi Yu
Supervision: William Randel
Validation: William Randel, Yunqian Zhu, Simone Tilmes, Jon Starr
Visualization: Jon Starr
Writing – original draft: William Randel
Writing – review & editing: William Randel, Yunqian Zhu, Simone Tilmes, Jon Starr, Wandi Yu, Rolando Garcia, Owen B. Toon, Mijeong Park, Douglas Kinnison, Jun Zhang, Adam Bourassa, Landon Rieger, Jianghanyang Li

stratospheric aerosol evolution (Zhu et al., 2022). As with the H_2O, HTHH aerosols have persisted and dispersed in the SH stratosphere; a notable feature is the separation of the H_2O and aerosol plumes over time due to sedimentation of the aerosols (Legras et al., 2022).

It is anticipated that the large H_2O and aerosol perturbations can impact stratospheric temperatures, circulation and chemistry. Substantial stratospheric warming has been observed linked to enhanced aerosols from the eruptions of El Chichón and Pinatubo (e.g., Angell, 1997; Labitzke & McCormick, 1992). While there are no precedents for the large H_2O perturbation in the observational data record, it is expected that increased H_2O will radiatively cool the stratosphere (e.g., Forster et al., 1999; Sellitto et al., 2022). Changes to stratospheric ozone (and related trace species) are also expected from large volcanic eruptions due to enhanced aerosol surface areas for heterogeneous chemistry, for example, Hofmann and Solomon (1989). In this paper we aim to document the observed changes in stratospheric climate and ozone during 2022 and early 2023, which are identified as large changes from climatology based on the past two decades. We furthermore run an ensemble of chemistry-climate model simulations using realistic HTHH inputs of H_2O and SO_2 to quantify impacts on stratospheric climate and chemistry, and evaluate their significance compared to internal variability. We first examine the detailed dispersion and evolution of the H_2O and aerosol plumes as observed and as simulated with WACCM to quantify the associated transport and radiative effects. We then compare modeled effects on circulation and ozone with observed anomalies in 2022. Similar behaviors are found in many regards, and these results can be used as fingerprints of HTHH effects on the stratosphere.

2. Observational Data and Model Experiments

2.1. Satellite Data

2.1.1. Microwave Limb Sounder (MLS)

The MLS instrument was launched onboard the EOS Aura satellite in 2004 as part of the "A-Train" satellite constellation and has operated continuously since that time in a low-Earth, high-latitude, sun-synchronous orbit. The instrument utilizes five broad microwave spectral regions, with centers ranging approximately from 118 to 2500 GHz, in a limb-viewing configuration to measure various atmospheric properties and constituents, including temperature, H_2O, O_3 and N_2O. For this work, version 5.0 of MLS H_2O, O_3, and temperature data (Livesey et al., 2020; Waters et al., 2006) were compiled into daily zonal means at a resolution of 2.5° latitude. The vertical resolution of temperature changes with pressure, ∼3–4 km for 100-10 hPa, ∼5–6 km up to 0.01 hPa, and 8–10 km above. The vertical resolution of the H_2O retrievals is ∼3 km, covering pressure levels 316 hPa to above 1 hPa. Anomalies for 2022 are calculated as deviations from the 2004–2021 background, and we especially highlight anomalies that are outside of all previous variability.

2.1.2. Ozone Monitor and Profiler Suite Limb Profiler (OMPS-LP)

Aerosol extinction and stratospheric aerosol optical depth (sAOD) data are from the University of Saskatchewan (USASK) Ozone Monitor and Profiler Suite Limb Profiler product (Bourassa et al., 2023). These data, derived from a tomographic inversion, provide height-resolved aerosol extinction at 745 nm with a tomographic inversion, with a vertical resolution of 1–2 km. The tomographic product improves vertical resolution and reduces artifacts from spatially inhomogeneous aerosols. However, the retrieval relies on assumed aerosol size and optical properties that may cause biases and large uncertainties during periods of enhanced aerosol.

2.2. The Fifth Generation of European ReAnalysis (ERA5)

Stratospheric circulations are derived using monthly European Center for Medium-Range Weather Forecasts ERA5 reanalysis data on model pressure levels (Hersbach et al., 2020). We include analyses of zonal winds, along with derived residual mean meridional circulation and Eliassen-Palm (EP) fluxes (Andrews et al., 1987). Anomalies in 2022 are calculated as deviations from the 2004–2021 climatology. We note that the ERA5 assimilation model did not include anomalous stratospheric H_2O or aerosols from HTHH, and hence the model is not balanced and likely incorporates large assimilation increments. This behavior is shown for a different assimilation model in Coy et al. (2022).

2.3. WACCM Chemistry-Climate Model Experiments

We use the Community Earth System Model, version 2 (CESM2), with the Whole Atmosphere Community Climate Model (WACCM) (Gettelman et al., 2019) as the atmosphere component, to simulate the stratospheric

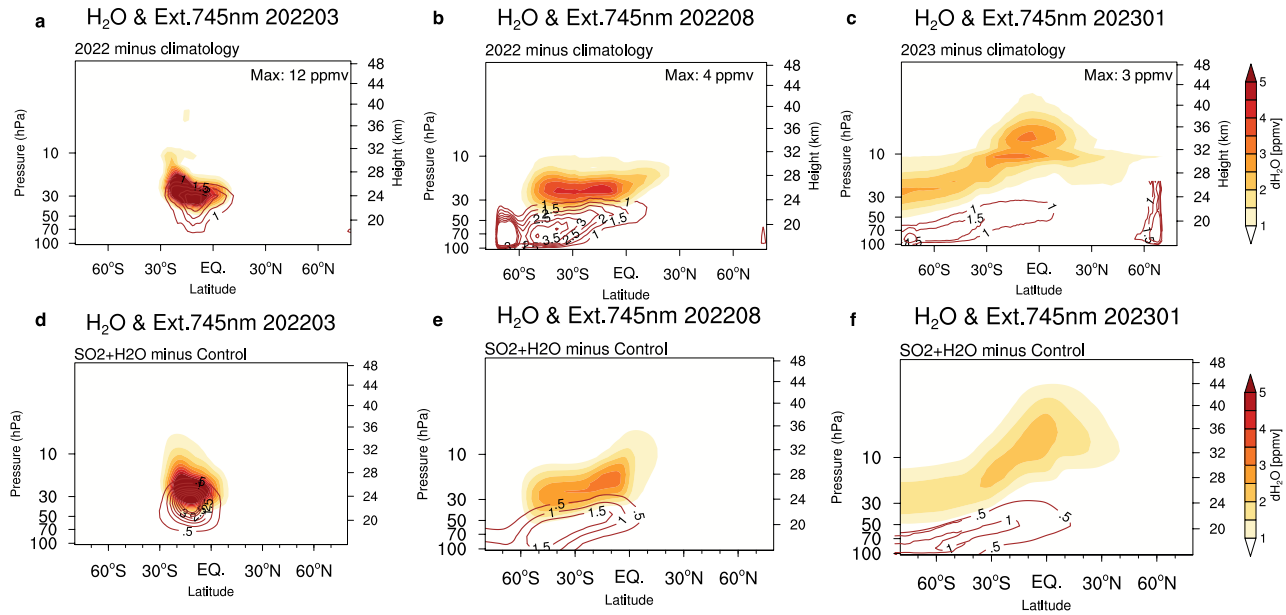

Figure 1. Observed and simulated H_2O and aerosol perturbations after the HTHH eruption. Panels (a–c) show the observed dispersion of the HTHH H_2O (colors, ppmv) enhancement and aerosol extinction (red contours, 10^{-3} km^{-1}) in (a) March, (b) August 2022 and (c) January 2023. The maximum H_2O amounts are indicated by the number on the top right corner; (d–f) are similar to (a–c) but for WACCM simulations.

H_2O and aerosol enhancements due to the HTHH eruption and evaluate their influence on stratospheric temperature, circulation and ozone chemistry. WACCM has 70 vertical layers extending upward to 140 km with vertical resolution of about 1–1.5 km in the stratosphere. The model is fully coupled to interactive ocean, sea-ice, and land models, and is initialized at the beginning of January 2022 using the observed sea-surface temperatures following the procedure described in Richter et al. (2022). The HTHH volcanic H_2O (~150 Tg) and SO_2 (~0.42 Tg) are injected on 15 January 2022 from ~20 to 35 km. The SO_2 injection is tuned based on comparisons between the simulated sulfate aerosol and OMPS Limb Profile aerosol extinction. The H_2O injection is tuned to mimic the observed MLS water vapor profile. More details can be found in Zhu et al. (2022). To accurately simulate the early plume structure and evolution, WACCM winds and temperatures are nudged to the Goddard Earth Observing System (GEOS) Modern-Era Retrospective Analysis for Research and Applications, Version 2 (MERRA–2) meteorological analysis (Gelaro et al., 2017) throughout January 2022; that is, the model is artificially constrained a model by adding a forcing term that relaxes its winds and temperatures toward the MERRA2 data with a 12-hr relaxation time scale. After 1 February 2022 the model is free-running to simulate fully-coupled variability including the coupling between changes in composition and radiation. We conducted four sets of experiments: the control case without SO_2 or H_2O (no volcanic forcing); an SO_2 only case with only SO_2 injection (with SO_2 converting to sulfate aerosol); an H_2O only case with only H_2O injection, and the $SO_2 + H_2O$ case with both SO_2 and H_2O injection, which mimics the total forcing of HTHH eruption. Calculated anomalies are the differences between the forcing runs and the control runs. We include 10 ensemble members for each scenario to examine internal variability and to better isolate forced behavior. Individual ensemble members differed by the last date of the meteorological nudging, in the range from 27 January 2022 to 5 February 2022. Once the nudging period ends, the model is free-running.

3. Results

3.1. Observed and Simulated Volcanic Plumes

Satellite observations show that the HTHH H_2O and aerosol plumes have persisted in the stratosphere and evolved throughout 2022 and early 2023 (Figures 1a–1c). The majority of the sulfate aerosol was initially collocated with the H_2O plume near 24 km (March 2022 in Figure 1a), but has subsequently sedimented to the lower stratosphere (Legras et al., 2022; Schoeberl et al., 2022) and dispersed in latitude to span much of the Southern Hemisphere (SH) by midwinter (August 2022 in Figure 1b). As a note, it is unclear from the OMPS extinction measurements

in Figure 1b whether the HTHH aerosols penetrated the Antarctic polar vortex, as the enhanced polar extinction in OMPS-LP measurements is also due to the formation of polar stratospheric clouds in this season. The H_2O plume was centered near 25 km and covered 60°S–20°N by August 2022; the H_2O anomalies (>4 ppmv in Figure 1b and >3 ppmv in Figure 1c) are large compared to the stratospheric background mixing ratio of ∼5 ppmv. By January 2023, the H_2O plume ascended in the tropical stratosphere and spread into the Northern Hemisphere midlatitudes (and over the pole in the SH) while the aerosol layer became weaker and remained over the SH lower stratosphere (Schoeberl et al., 2023).

The modeled evolution of the H_2O and sulfate aerosol plumes in the $SO_2 + H_2O$ case are shown in Figure 1d–1f, with patterns similar to those observed. Results in Figures 1d–1f are ensemble averages, but there are relatively small differences in the evolution of the plumes among the 10 realizations (not shown). The H_2O and aerosol plumes initially overlap and then separate vertically over time, with latitudinal dispersion similar to the observed behavior. The model HTHH aerosol layer in the lower stratosphere extends to polar latitudes near the bottom of the polar vortex during winter (Figure 1e), while the H_2O plume spreads poleward but is mostly excluded from polar latitudes by the stronger jet near 25 km (see discussion in Section 3.3). The magnitude of the model aerosol extinction in midwinter is about half as large as measured by OMPS-LP (cf. Figures 1b–1e), which may be related to uncertainties in SO_2 injection amount and/or the modeled aerosol size distribution and evolution, along with uncertainties in the OMPS-LP retrievals.

The HTHH aerosol plume descends over time and disperses meridionally in the SH lower stratosphere. Details of the latitudinal distribution of sAOD observed during 2022 by OMPS are shown in Figure 2a, suggesting a double-peak sAOD pattern in latitude, with one tropical maximum associated with immediate aerosol formation and one midlatitude maximum during SH winter (∼July-September). The double-peak sAOD was also reported from observation and model simulation of the 1991 Pinatubo eruption (Long & Stowe, 1994; Quaglia et al., 2023) and from the response of sustained SO_2 injections under geoengineering (Tilmes et al., 2017). The pattern arises as aerosols spread rapidly across the surf zone into the SH midlatitudes during winter, resulting in a lower sAOD in between. Then the sAOD accumulates in mid-latitudes as the SH polar vortex constitutes a transport barrier. This behavior is qualitatively captured in the WACCM $SO_2 + H_2O$ model simulations (Figure 2b), although the midlatitude sAOD in the model is about half as large as observed. One possible reason is that the model underestimates the aerosol particle effective radius compared with that in SAGE III/ISS (Khaykin et al., 2022) due to either inadequate model microphysics processes or unconsidered pre-existing particles such as sea salt.

The large perturbations of stratospheric H_2O and aerosol have substantial effects on the solar and infrared radiation balances, which in turn influence stratospheric temperatures and circulation. The radiative impacts of H_2O and aerosol volcanic plumes simulated in WACCM are estimated from the instantaneous radiative heating rates (i.e., longwave heating rate plus shortwave heating rate, without dynamical or thermal adjustment) due to volcanic plumes, as shown in Figure 3 for August 2022. Specifically, the water vapor and sulfate aerosols from the volcanic run are imposed on the no-volcano run, and the shortwave and longwave heating rates are calculated and output after one model time step, before any thermal or dynamical feedbacks have occurred. The H_2O plume produces a localized cooling of order −0.1 K/day that overlaps the plume, while a small heating layer occurs near the bottom due to upwelling longwave radiation (Figure 3b). A small net aerosol radiative heating overlaps the aerosol plume (Figure 3c), reinforcing the warming below the H_2O plume, so that there is a dipole vertical structure of cooling above warming for the combined effects (Figure 3a). The calculated forcings are almost completely due to longwave effects. Instantaneous radiative heating/cooling rate patterns are similar in other months (not shown), and decrease slowly over time as the plumes disperse.

3.2. Temperature Perturbation

Satellite observations show evidence of systematic stratospheric cooling following the HTHH eruption (Figures 4a and 4b). Temperatures near 25 hPa over the SH show cold anomalies in 2022 that are well outside of previous variability, beginning one-to-two months after the eruption (Figure 4a). This delay is consistent with a radiative response to the increased H_2O near this altitude with a radiative time scale of ∼10–20 days (e.g., Hitchcock et al., 2010). The vertical structure of the temperature anomalies averaged over 60°S–10°S (Figure 4b) shows cooling covering much of the mid-stratosphere throughout 2022, with largest cold anomalies during SH winter (June-August) extending to ∼45 km. During these months there are anomalous warm temperatures in the lower mesosphere above ∼50 km (Yu et al., 2023, see Section 3.3). Cold anomalies are reduced in 2023.

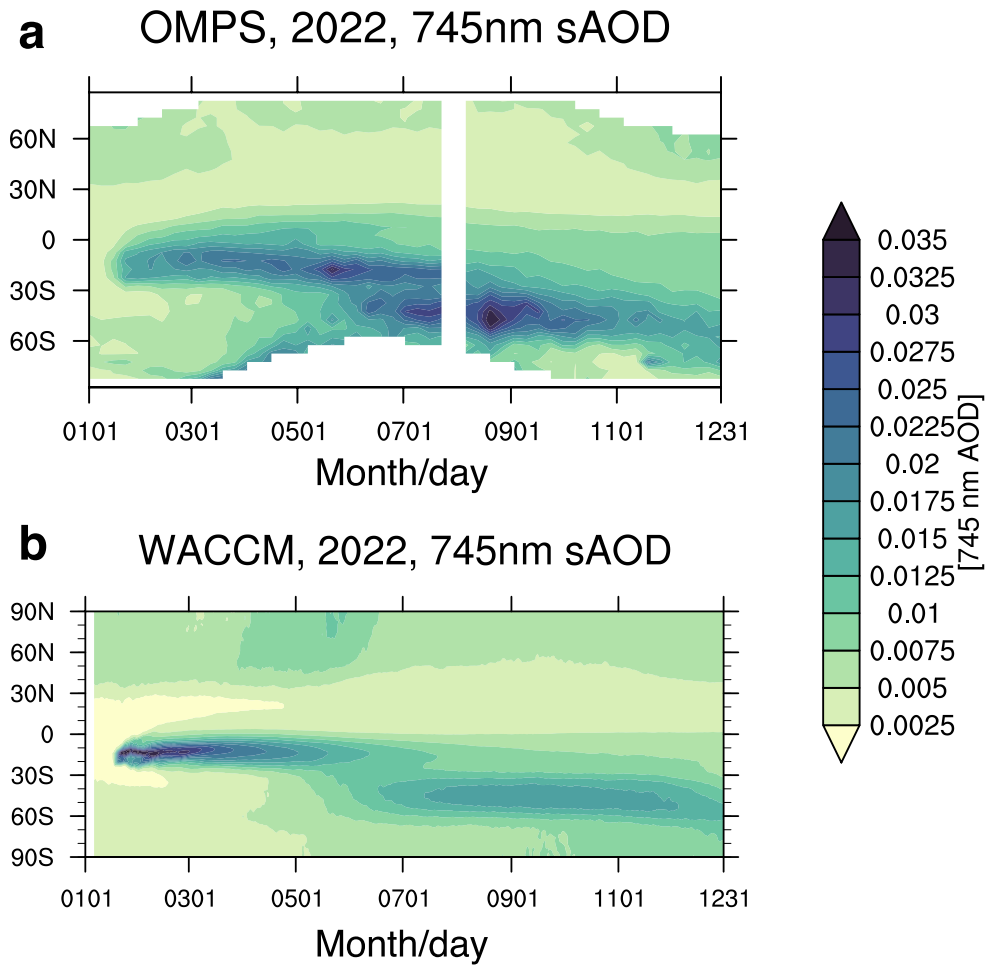

Figure 2. Latitude-time plots of the zonal average stratospheric aerosol optical depth at 745 nm in 2022 from (a) OMPS-LP and (b) WACCM ensemble $H_2O + SO_2$ ensemble average. Both panels show total aerosol optical depth, not anomalies.

The unprecedented evolution of temperatures in 2022 suggests forced changes from the HTHH eruption, but also contains components of internal variability. To evaluate the forced signal in the model runs we use ensemble simulations of WACCM with and without the volcanic injections. The modeled structure of temperature changes in the ($H_2O + SO_2$) simulations (Figures 4c and 4d) capture the salient aspects of the observed behavior including

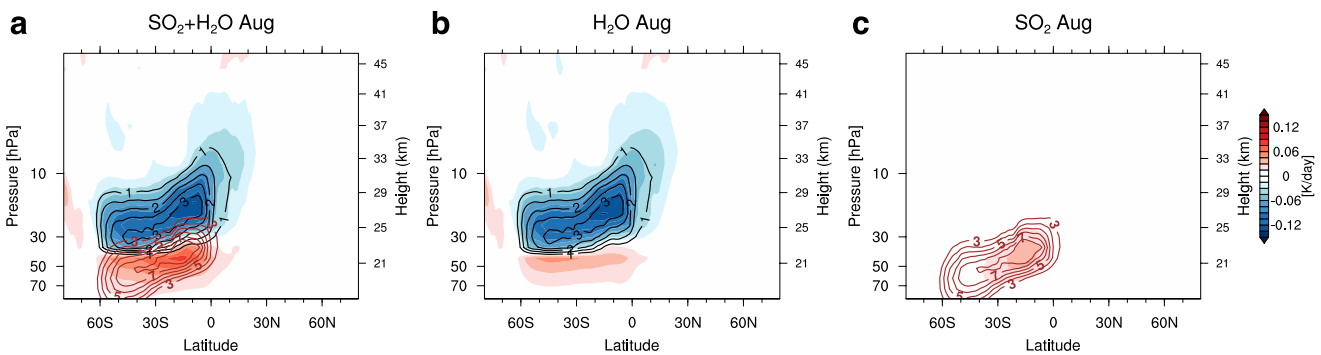

Figure 3. August net radiative heating rate (longwave plus shortwave tendencies, colors, unit: K/day) due to (a) both H_2O and aerosol plumes, (b) H_2O plume only, and (c) sulfate aerosol plume only, compared to no-forcing control runs. Red line contours denote the sulfate aerosol mixing ratio in ppbm, and black line contours denote the anomalous H_2O concentration in ppmv.

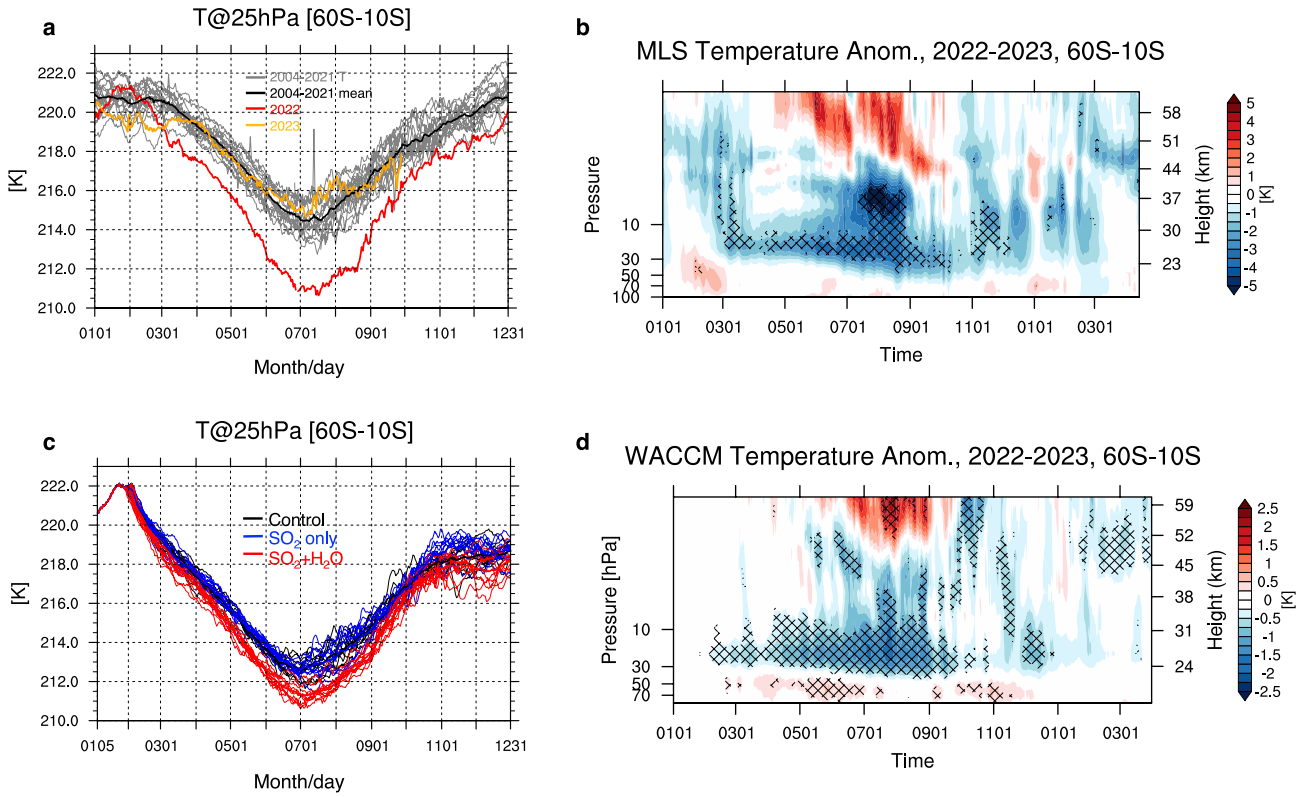

Figure 4. Temperatures averaged over 60°S–10°S from MLS observations showing persistent anomalous cooling in 2022. (a) Gray lines show time series of MLS temperatures at 25 hPa for 2004–2021 while the black line is the climatology. Red/orange lines shows 25 hPa temperature for 2022/2023. (b) Time-height section of MLS temperature anomalies (differences from 2004 to 2021 averages). Hatched regions in (b) indicate where the 2022 anomalies are outside the range of all variability during 2004–2021. (c) As in (a), but temperatures at 25 hPa simulated in WACCM. Black lines indicate the control cases, blue lines indicate SO_2 only cases, and red lines indicate the $SO_2 + H_2O$ cases, respectively (including 10 realizations for each case). (d) Time-height section of WACCM temperature differences for the $SO_2 + H_2O$ minus control ensemble means. Hatched regions indicate where the temperature anomalies are statistically significant at the 95% level according to Student's *t*-test. Note that color bars in (b) and (d) have different ranges.

cooling throughout the year over ~25–30 km and enhanced winter maxima, including warming in the lower mesosphere (Figure 4d).

Observed cold temperature anomalies and H_2O plume overlap until April and decouple in early SH winter. The strongest cooling occurs primarily in midlatitudes centered near 50°S, and do not directly overlap the H_2O plume as illustrated for August 2022 in Figure 6a (other months are shown in Figure S1 in Supporting Information S1). High latitude cold anomalies (in excess of 15 K) occur in combination with warm tropical anomalies, with maxima near 23 and 38 km. Part of the tropical and extratropical temperature maxima are related to the phase of the Quasi-Biennial Oscillation (QBO) in 2022 (Coy et al., 2022). The see-saw patterns in temperature (opposite sign responses) between high and low latitudes are suggestive of coupling to the hemispheric-scale mean meridional circulation (Yulaeva et al., 1994). The strong high latitude temperature anomalies are in balance with changes in the stratospheric circulation, as discussed below.

The simulated ensemble average temperature changes in response to the ($SO_2 + H_2O$) forcing in August are shown in Figure 5b (other months are shown in Figure S2 in Supporting Information S1); they display patterns similar to observed behavior (Figure 5a, Figure S1 in Supporting Information S1), although the model winter cooling is centered at somewhat higher latitudes (60–70°S). Modeled temperature changes with only SO_2 (sulfate aerosol) forcing (Figure 5c) have temperature perturbations of similar polarity to the total forcing (tropical warming and high latitude cooling), but are weaker and not significant (see also blue lines in Figure 4c). Without H_2O injection the volcanic aerosol layer is thicker and heats the lower stratosphere over a deeper vertical layer, implying that the coupled H_2O-aerosol effects have amplified stratospheric cooling in the high latitudes. In contrast, simulations with only H_2O injection show a very different temperature response (Figure 5d), with weak cooling anomalies in

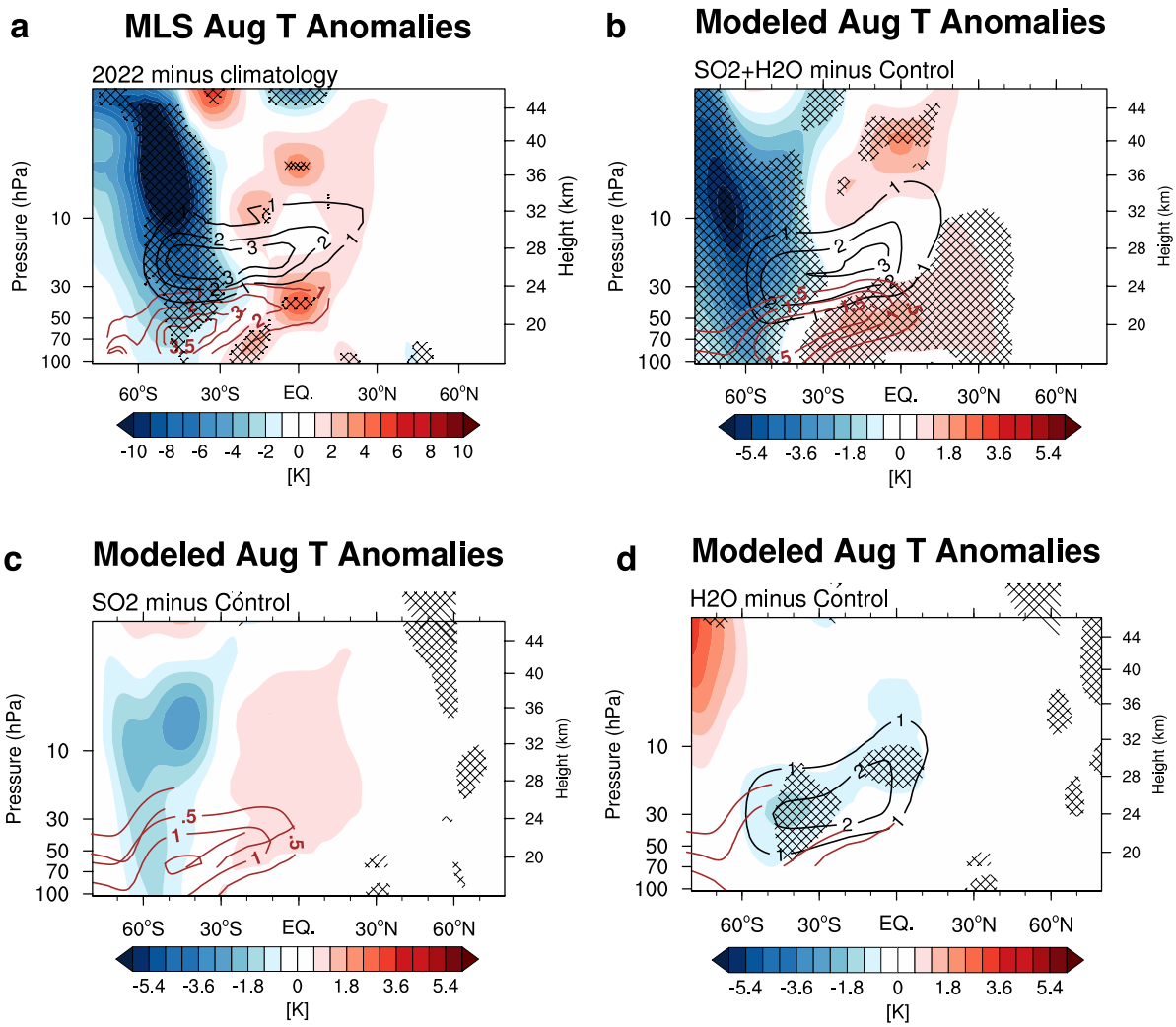

Figure 5. Observed and modeled temperature anomalies in August 2022 (color shading, K). (a) MLS observations, calculated as differences between the 2022 and the 2004–2021 average. (b) WACCM simulated modeled temperature changes in the all-forcing (SO_2 + H_2O) case minus the no-forcing control runs. (c) Similar to (b), but for SO_2 only simulations. (d) Similar to (b), but for H_2O only simulations. Red line contours denote the sulfate aerosol extinction in 10^{-3} km^{-1}, and black line contours denote the anomalous H_2O concentration in ppmv. Hatched regions denote statistical significance, as in Figure 4.

the tropics and midlatitudes that overlap the H_2O plume. The responses due to the single-forcing H_2O and SO_2 perturbations are not additive. Overall, our model sensitivity experiments demonstrate that stratospheric temperature responses change from direct radiative effect in the early stage to much stronger dynamical effect during SH winter. Including both H_2O and SO_2 (sulfate aerosol) forcings is important for realistic simulation of the HTHH responses with strong effects only for the combined forcings.

The coupling of stratospheric temperature (polar vortex strength) and planetary wave amplitude is a well-known feature of the winter stratosphere, with correlation between wave amplitudes and polar temperature (e.g., Andrews et al., 1987; Holton & Mass, 1976; Randel & Newman, 1998). The coupling is evident in Figure 6 as correlations of polar temperature versus planetary wave activity (quantified as the vertical component of the Eliassen-Palm flux divergence in the lower stratosphere) for our control simulations, showing results for July and August for each of the 10 realizations. Figure 6 furthermore shows a systematic shift in temperatures and wave activity in the H_2O + SO_2 forced run with respect to the control runs, with colder temperature and weaker Eliassen-Palm (EP) fluxes associated with the HTHH forcing in most cases. We view this shift as a fingerprint of the forced response due to the HTHH forcing. While most of the H_2O + SO_2 ensemble members show relative cold temperatures and weak wave fluxes, there is considerable stochastic variability among the realizations, and several realizations

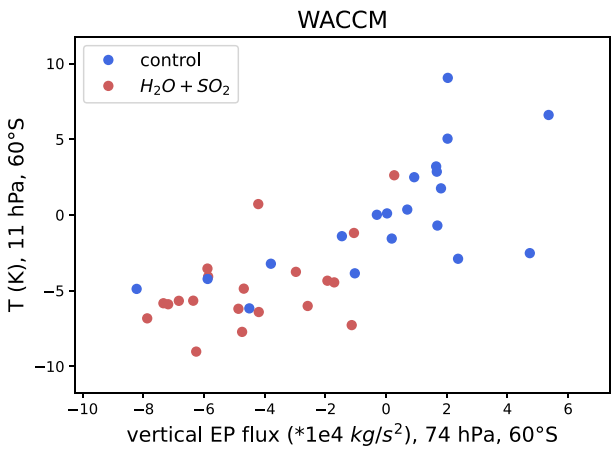

Figure 6. The relationship between temperatures at 60°S, 10 hPa and the vertical component of EP flux divergence at 60°S, 74 hPa in the WACCM control (blue) and $H_2O + SO_2$ (red) simulations. Results are shown for both July and August statistics for the 10 realizations in each ensemble.

(6 out of 10) have temperature anomalies comparable to the observed 2022 anomalies. We conclude that internal variability in the ensemble model simulations contributes to the low bias in ensemble average temperature anomalies in Figure 4 compared to the observed pattern in 2022 (Yu et al., 2023). In spite of this difference in magnitude, the similarity in timing and spatial structure of observed and modeled temperature patterns is strongly suggestive of an HTHH attribution for the observed anomalies.

3.3. Stratospheric Circulation Response

Because they are in thermal wind balance with the temperature anomalies, the zonal mean zonal winds show intensification and equatorward shift of the polar vortex throughout the winter (see Figure 7a for August). The simulated zonal wind changes also show a strengthening and equatorward shift of the winter westerlies in response to the (SO_2 + H_2O) forcing (Figure 7b), with patterns similar to the observed anomalies. As with temperatures, the model ensemble mean wind anomalies are only about half as large as observed in 2022. Reanalysis fields and models show that the strengthened polar vortex persists into SH spring (Figures S3 and S4 in Supporting Information S1). Figures 7a and 7b also include anomalies in the residual mean meridional (Brewer-Dobson) circulation (BDC), highlighting anomalous high latitude upwelling and low latitude downwelling that opposes and weakens the normal background equator to pole circulation. These results are consistent with the residual circulation anomaly patterns discussed in Coy et al. (2022) and the weakened background tropical upward residual circulation in Schoeberl et al. (2022). The changes in the BDC are associated with adiabatic cooling/warming in stratosphere/mesosphere, and are also consistent with weakened planetary-scale wave forcing in the middle and upper stratosphere. As noted above (Figure 5), the SO_2 + H_2O simulations have planetary wave amplitudes and EP fluxes that are about half the size of the control runs, and reanalysis data likewise show weak planetary waves in 2022. We note that the vertical out-of-phase temperature changes above ~50 km observed in winter (Figures 4b–4d) are characteristic of dynamically forced effects, consistent with the reductions in stratospheric EP fluxes (Andrews et al., 1987). Similar to differences in temperature response (Figure 6), model simulations with only sulfate aerosol forcing or only H_2O forcing show mostly insignificant circulation changes (Figure S5a in Supporting Information S1) or opposite circulation responses (Figure S5b in Supporting Information S1) across 10 ensembles, highlighting the importance of combined effects due to sulfate aerosol and H_2O enhancements.

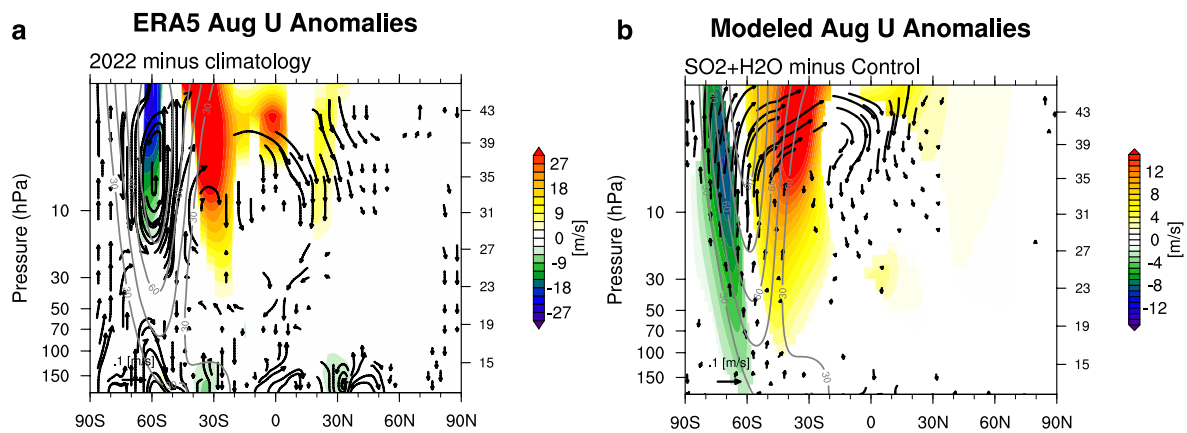

Figure 7. Anomalous zonal wind changes in August 2022. Colors show zonal mean zonal wind anomalies in (a) observations from the ERA5 reanalysis data and (b) simulations in the all-forcing (SO_2 + H_2O) WACCM simulations compared to the control runs. Gray contours show the background zonal winds with an interval of 15 m/s. Colored regions in (a) indicate where the 2022 anomalies are outside the range of all variability during 2004–2021. The vectors depict anomalies in the residual mean meridional circulation (BDC) in ERA5 that are outside of two standard deviations. Colored regions and vectors in (b) indicate where anomalies are significant at the 95% level.

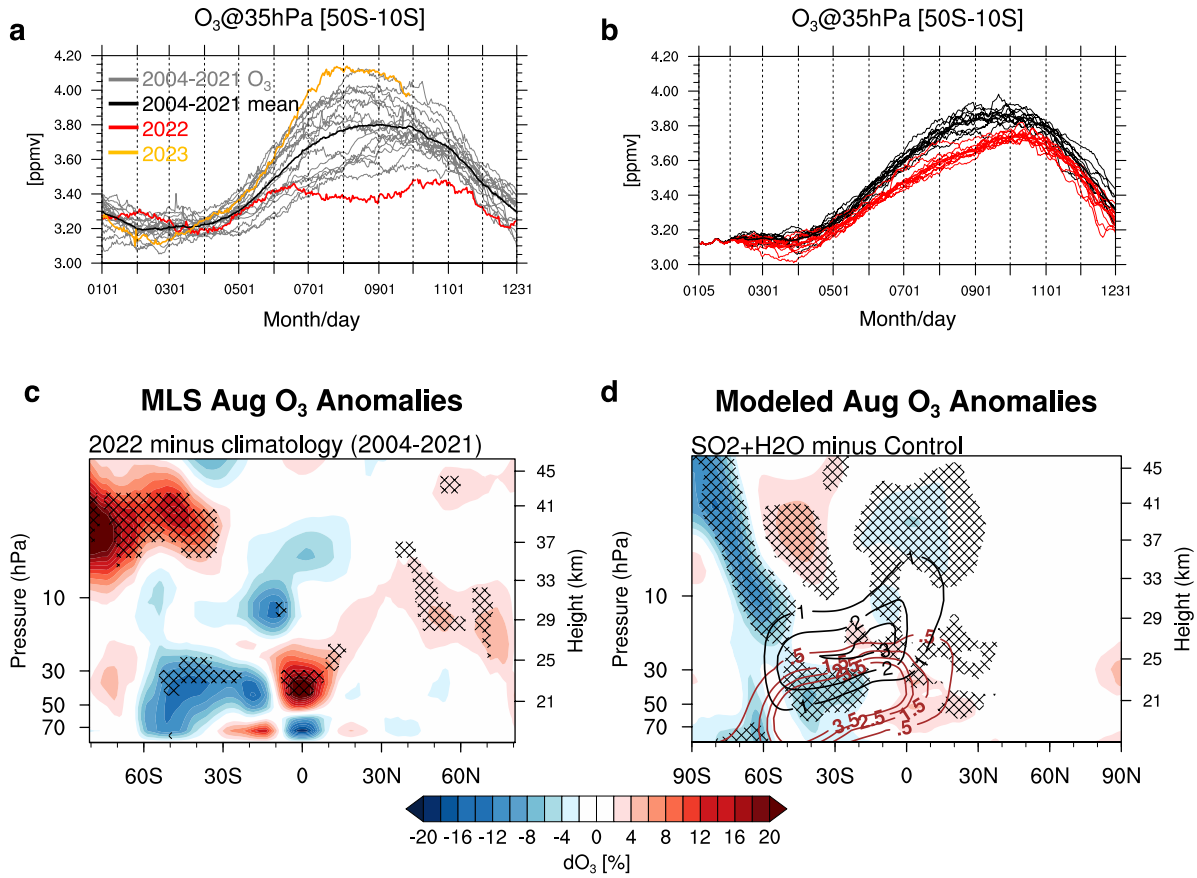

Figure 8. Evolution of midlatitude stratospheric ozone after HTHH. (a) Time series of MLS observed ozone (in ppmv) at 35 hPa, 50°S–10°S, showing low ozone values in 2022 (red line) compared to other years. Gray lines show time series for 2004–2021, the black line is the climatology, and the orange line shows 35 hPa ozone for 2023. (b) Ozone at 35 hPa simulated in WACCM, comparing the control cases (black lines) and the SO_2 + H_2O cases (red lines). Fractional ozone anomalies (color shading, %) from (c) MLS and (d) WACCM simulation in August 2022. Regions of significant changes are hatched, as in Figure 4.

3.4. Midlatitude Stratospheric Ozone Changes

Stratospheric ozone changes after HTHH can be anticipated from both changes in circulation and anomalous chemistry from enhanced H_2O and aerosols (Hofmann & Solomon, 1989; Lu et al., 2023; Solomon, 1999; Tie & Brasseur, 1995; Yook et al., 2022; Zhu et al., 2022). MLS observations show lower stratospheric (LS) ozone reductions during winter over the SH midlatitudes and tropics (~50°S–10°S), which are outside of previous variability (Figure 8a). The lower stratospheric midlatitude ozone decreases are accompanied by anomalously high values over the equator (Figure 8c), and part of these coupled anomalies are linked to the phase of the QBO in 2022 (Schoeberl et al., 2023). We note that midlatitude QBO anomalies in ozone often have an asymmetric latitude structure with maximum amplitude in the winter hemisphere (Randel et al., 1999), as observed here. This QBO influence can be seen in the relatively large spread of midlatitude winter ozone amounts in 2004–2021 seen in Figure 8a, with individual years typically above or below the long-term mean, but note that low values in 2022 extend outside of this background variability. The wintertime SH mid-latitude ozone reduction is reproduced in the model (Figures 8b and 8d, below 30 hPa), with similar spatial and temporal patterns to those observed, but only about half the anomaly magnitude in the ensemble average. Note the lack of strong interannual variations in the individual model realizations in Figure 8b, due to a lack of subtropical QBO variability in these idealized model simulations (all 10 realizations are initialized with the same phase of the QBO). The large difference in ozone response between MLS and WACCM in the upper stratosphere (above 30 hPa, poleward of 60°S) is consistent with the streamfunction anomalies shown in Figure 7, which are computed from the values in 2022 minus climatology in MLS and from the 2022 volcano minus no volcano simulations in WACCM.

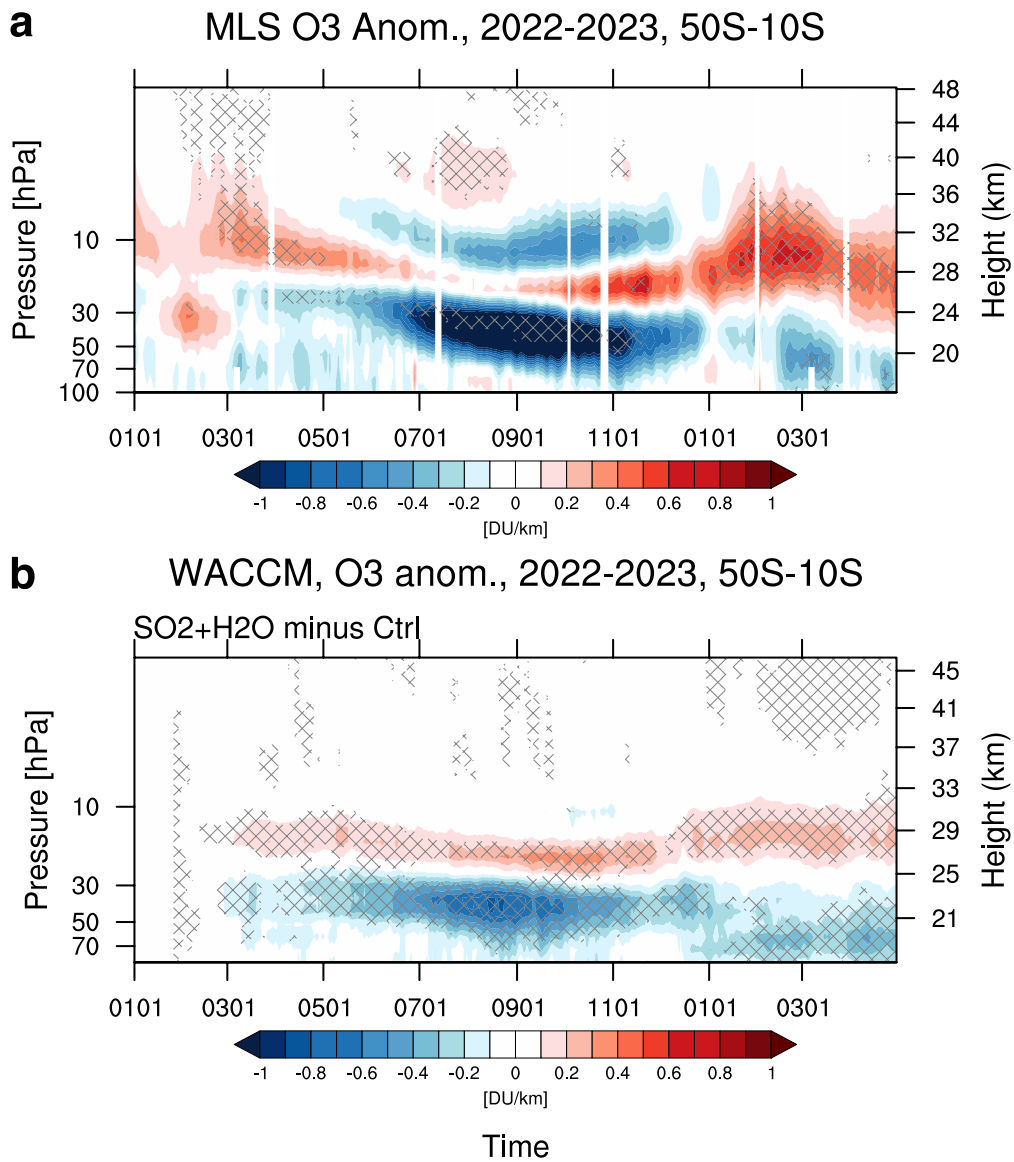

Figure 9. Time-height sections of ozone density anomalies (units: DU/km) averaged over 10–50°S, showing results from (a) MLS observations and (b) WACCM model simulations (ensemble average $SO_2 + H_2O$ minus control). Hatched regions denote significance, as in Figure 4.

The evolution of SH midlatitude ozone changes associated with HTHH is highlighted in Figure 9, which shows density-weighted ozone anomalies (in DU/km) over 50°–10° S from MLS data and WACCM $SO_2 + H_2O$ simulations. Observations show strong negative anomalies in the lower stratosphere that maximize during winter, and similar but weaker patterns are found in the model ensemble mean. There is a narrow layer of ozone increases above the lower level decreases seen in both observations and model in Figures 8a and 8b persisting through May 2023. The center or node of this vertical dipole pattern coincides in altitude with the climatological ozone maximum near 25 km, so that these ozone changes are consistent with the weakening of the midlatitude BDC discussed above. The consistency on the timing of circulation changes and LS ozone losses, which both maximize during SH winter (e.g., temperature anomalies in Figure 4 and ozone losses in Figures 8 and 9), is a fingerprint of substantial contribution due to changes in transport. This aligns with the conclusion in Santee et al. (2023) that no appreciable chemical ozone loss occurred in SH midlatitude. We note that while ozone changes in the $SO_2 + H_2O$ WACCM simulations result from a combination of transport and chemistry effects, it is not simple to

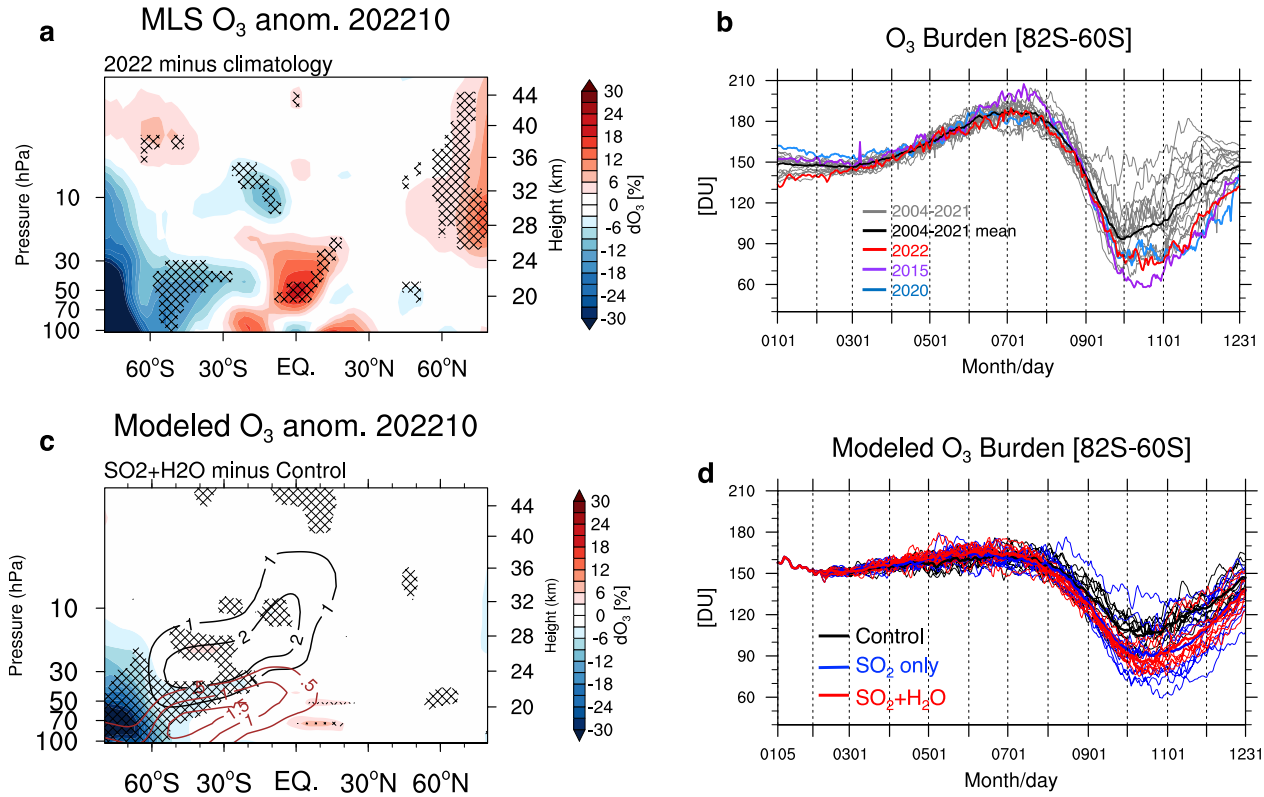

Figure 10. (a) Fractional ozone anomalies (%) from MLS in October 2022. Hatched regions indicate where the 2022 anomalies are outside the range of all variability during 2004–2021. (b) MLS observations of polar cap (82°S–60°S) ozone column over 11–22 km in 2004–2022. (c) Similar to (a) but modeled October ozone changes in $SO_2 + H_2O$ minus control simulations. Hatched regions mark the grid points for which the changes exceed the 95% significance level according to Student's *t*-test. (d) Similar to (b) but corresponding modeled results comparing control, $SO_2 + H_2O$ and SO_2 only simulations.

separate dynamical and chemical contributions in our coupled simulation. Complementary studies using Specified Dynamics WACCM (SD-WACCM) may help quantify the importance of the different chemical and dynamical processes affecting the midlatitude ozone loss (Zhang et al., 2023).

3.5. Antarctic Stratospheric Ozone

Anomalous ozone changes during 2022 are also found associated with the Antarctic ozone hole (Figures 10a and 10b), where variability is tied to polar stratospheric cloud (PSC) and aerosol amounts together with cold temperatures that generate photochemically active chlorine (Solomon et al., 1986; Zhu et al., 2017). In the model, springtime polar ozone losses are enhanced by HTHH aerosols that reach the polar stratosphere (red contours in Figure 10c), in combination with anomalously cold temperatures from circulation effects that enhance reactive chlorine chemistry. The combined effects of $SO_2 + H_2O$ lead to net losses of ~15 DU compared to control runs amid substantial variability in the polar region (Figure 10d), and comparisons with SO_2 only simulations (blue lines in Figure 10d) show that most of the polar ozone losses are due to the impact of HTHH aerosols. Time series in Figure 9d show that the ozone loss rates accelerate in September, during the formation of the ozone hole. MLS observations show a relatively deep ozone hole in October 2022 (Figures 10a and 10b), but differences with previous years are only apparent during and after October; this detail is different from the model behavior, where differences are already noticeable in September. The bias may come from comparing the anomaly from 2004 to 2021 climatology versus the anomaly from control runs. We note that, while the HTHH aerosols penetrated across the bottom of the polar vortex and provided more surface area to promote heterogenous chemistry in the model (Figure 1e), it is unclear if this behavior occurred in the real atmosphere because enhanced polar aerosol extinction in the OMPS data (e.g., Figure 1b) could simply reflect the occurrence of polar stratospheric clouds. In any case, the observed Antarctic ozone remains near record low levels during SH spring (October-December

in Figure 10b), rivaling other recent years with enhanced polar aerosols due to volcanic eruptions such as the Calbuco volcanic eruption in 2015 (purple line in Figure 10b, Solomon et al., 2016; Stone et al., 2017; Zhu et al., 2018) and smoke from wildfires (blue line in Figure 10b, Australian bush fires in 2020 persisting into 2021; Rieger et al., 2021).

4. Conclusion

Satellite measurements demonstrate persistent perturbations in stratospheric temperatures and circulation following the HTHH eruption, including influences on the seasonally-evolving polar vortex, planetary waves and Brewer-Dobson circulation. Global chemistry-climate model simulations forced by HTHH inputs can track the evolving H_2O and aerosol plumes, and the modeled volcanic responses in temperatures and circulation in the SH are similar to the time-evolving patterns of the observed behavior. This agreement suggests that the observed stratospheric changes are a fingerprint of the forced global-scale response to the HTHH eruption. Several realizations have strong responses in temperature and circulation as large as that observed in 2022, however, the ensemble average forced model responses are only about half the magnitude of observed anomalies in 2022. These differences are likely related to large stochastic variability due to wave-mean flow coupling during SH winter, evident in model simulations (Figure 6) and are not negligible compared to the HTHH forcing. Comparison of control and HTHH model results (Figure 6) suggests that the HTHH forcing biases pushed the system toward a balance of weak wave fluxes and a cold/strong polar vortex, although the dynamical details are not well understood. Sensitivity experiments further demonstrate that the combined effects of both H_2O and SO_2 (sulfate aerosol) are important in these simulations, as smaller and insignificant changes are found in individual H_2O or SO_2 forcing experiments.

MLS observations show anomalous low ozone in the SH winter midlatitude lower stratosphere following HTHH; although some component of these low values is probably related to the phase of the QBO (as evidenced by out-of-phase changes over the equator), the low 2022 values are outside of all previous variability. The WACCM $SO_2 + H_2O$ simulations capture the key spatial and temporal patterns of these midlatitude ozone changes, arguing for an HTHH attribution of the observed low values. Large ozone decreases during 2022 are also found associated with the Antarctic ozone hole. While it is not simple to separate ozone changes due to transport and chemistry effects in our coupled model simulations, the spatial and temporal fingerprints suggest a dominant contribution from transport effects at midlatitudes, and from heterogeneous chemistry in the Antarctic. Future studies using models constrained with nudged meteorological fields may help separate the influence of chemistry from dynamics. The WACCM simulations show that aerosol transported to the Antarctic lower stratosphere combined with a circulation-induced cold polar vortex contributed to low Antarctic ozone levels in the model during September-December (i.e., a relatively deep ozone hole). Observed Antarctic ozone levels were relatively low during October-December 2022 (Figure 10b), consistent with the model behavior, although there is no evidence of anomalous amounts of reactive Cl species inside the vortex (Manney et al., 2023). The 2022 SH ozone losses caused by HTHH are transient effects and should not impact the long-term ozone recovery expected from the Montreal Protocol. In addition, the simulations show no significant sea surface temperature change between the all-forcing runs and the control runs across 10 ensembles until early 2023 (not shown). However, the sustained water vapor enhancement due to HTHH eruption might be expected to affect surface climate in the upcoming years. The HTHH eruption provides a remarkable natural experiment for validating a fully coupled chemistry-climate model and provides confidence in ensemble forecast simulations, such as those performed here.

Data Availability Statement

[Dataset] ERA5 meteorological products are available from the Copernicus Climate Data Store. See ERA5 (2023). [Software] CESM2/WACCM6 is an open-source community model, which was developed with support primarily from the National Science Foundation. See Gettelman et al. (2019).

Acknowledgments
This project received funding from NOAA's Earth Radiation Budget (ERB) Initiative (CPO #03-01-07-001). This research was supported in part by NOAA cooperative agreements NA17OAR4320101 and NA22OAR4320151, and by the NASA Aura Science Team under Grant 80NSSC20K0928. OBT was supported by NSF Award AGS 1853932. The work contribution of WY was performed under the auspices of the US Department of Energy (DOE) by Lawrence Livermore National Laboratory under contract no. DE-AC52-07NA27344. JZ is supported by the NSF via NCAR's Advanced Study Program Postdoctoral Fellowship. The authors thank Drs Nathaniel Livesey, Michelle Santee, Paul Newman, Holger Vömel, Karen Rosenlof, Robert Portmann, and Ewa Bednarz for helpful discussions. NCAR's Community Earth System Model project is supported primarily by the National Science Foundation. This material is based upon work supported by the National Center for Atmospheric Research, which is a major facility sponsored by the NSF under Cooperative Agreement No. 1852977. Computing and data storage resources, including the Cheyenne supercomputer (https://doi.org/10.5065/D6RX99HX), were provided by the Computational and Information Systems Laboratory (CISL) at NCAR.

References

Andrews, D. G., Holton, J. R., & Leovy, C. B. (1987). *Middle atmosphere dynamics*. Academic press.

Angell, J. K. (1997). Estimated impact of Agung, El Chichón and Pinatubo volcanic eruptions on global and regional total ozone after adjustment for the QBO. *Geophysical Research Letters*, *24*(6), 647–650. https://doi.org/10.1029/97gl00544

Bourassa, A. E., Zawada, D. J., Rieger, L. A., Warnock, T. W., Toohey, M., & Degenstein, D. A. (2023). Tomographic retrievals of Hunga Tonga-Hunga Ha'apai volcanic aerosol. *Geophysical Research Letters*, *50*(3), e2022GL101978. https://doi.org/10.1029/2022gl101978

Carn, S., Krotkov, N., Fisher, B., & Li, C. (2022). Out of the blue: Volcanic SO_2 emissions during the 2021-2022 Hunga Tonga-Hunga Ha'apai eruptions.

Coy, L., Newman, P. A., Wargan, K., Partyka, G., Strahan, S. E., & Pawson, S. (2022). Stratospheric circulation changes associated with the Hunga Tonga-Hunga Ha'apai eruption. *Geophysical Research Letters*, *49*(22), e2022GL100982. https://doi.org/10.1029/2022gl100982

ERA5. (2023). ERA5 monthly data on pressure levels from 1979 to present [Dataset]. ECMWF. https://doi.org/10.24381/cds.bd0915c6

Forster, F., Piers, M. D., & Shine, K. P. (1999). Stratospheric water vapour changes as a possible contributor to observed stratospheric cooling. *Geophysical Research Letters*, *26*(21), 3309–3312. https://doi.org/10.1029/1999gl010487

Gelaro, R., McCarty, W., Suárez, M. J., Todling, R., Molod, A., Lawrence, T., et al. (2017). The modern-era retrospective analysis for research and applications, version 2 (MERRA-2). *Journal of Climate*, *30*(14), 5419–5454. https://doi.org/10.1175/jcli-d-16-0758.1

Gettelman, A., Mills, M. J., Kinnison, D. E., Garcia, R. R., Smith, A. K., Marsh, D. R., et al. (2019). The whole atmosphere community climate model version 6 (WACCM6). *Journal of Geophysical Research: Atmospheres*, *124*(23), 12380–12403. https://doi.org/10.1029/2019jd030943

Hersbach, H., Bell, B., Paul, B., Hirahara, S., Horányi, A., Muñoz-Sabater, J., et al., (2020). The ERA5 global reanalysis. *Quarterly Journal of the Royal Meteorological Society*, *146*(730), 1999–2049. https://doi.org/10.1002/qj.3803

Hitchcock, P., Shepherd, T. G., & Yoden, S. (2010). On the approximation of local and linear radiative damping in the middle atmosphere. *Journal of the Atmospheric Sciences*, *67*(6), 2070–2085. https://doi.org/10.1175/2009jas3286.1

Hofmann, D. J., & Solomon, S. (1989). Ozone destruction through heterogeneous chemistry following the eruption of El Chichon. *Journal of Geophysical Research*, *94*(D4), 5029–5041. https://doi.org/10.1029/jd094id04p05029

Holton, J. R., & Mass, C. (1976). Stratospheric vacillation cycles. *Journal of the Atmospheric Sciences*, *33*(11), 2218–2225. https://doi.org/10.1175/1520-0469(1976)033<2218:svc>2.0.co;2

Jenkins, S., Smith, C., Allen, M., & Grainger, R. (2023). Tonga eruption increases chance of temporary surface temperature anomaly above 1.5° C. *Nature Climate Change*, *1–3*.

Khaykin, S., Podglajen, A., Ploeger, F., Grooß, J. U., Tencé, F., Bekki, S., et al. (2022). Global perturbation of stratospheric water and aerosol burden by Hunga eruption.

Labitzke, K., & McCormick, M. P. (1992). Stratospheric temperature increases due to Pinatubo aerosols. *Geophysical Research Letters*, *19*(2), 207–210. https://doi.org/10.1029/91gl02940

Legras, B., Duchamp, C., Sellitto, P., Podglajen, A., Carboni, E., Siddans, R., et al. (2022). The evolution and dynamics of the Hunga Tonga–Hunga Ha'apai sulfate aerosol plume in the stratosphere. *Atmospheric Chemistry and Physics*, *22*(22), 14957–14970. https://doi.org/10.5194/acp-22-14957-2022

Li, F., & Newman, P. (2020). Stratospheric water vapor feedback and its climate impacts in the coupled atmosphere–ocean Goddard earth observing system chemistry-climate model. *Climate Dynamics*, *55*(5), 1585–1595. https://doi.org/10.1007/s00382-020-05348-6

Livesey, N. J., Read, W. G., Wagner, P. A., Froidevaux, L., Santee, M. L., & Schwartz, M. J. (2020). *Version 5.0 x level 2 and 3 data quality and description document (Tech. Rep. No. JPL D-105336 Rev. A)*. Jet Propulsion Laboratory.

Long, C. S., & Stowe, L. L. (1994). Using the NOAA/AVHRR to study stratospheric aerosol optical thicknesses following the Mt. Pinatubo eruption. *Geophysical Research Letters*, *21*(20), 2215–2218. https://doi.org/10.1029/94gl01322

Lu, J., Lou, S., Huang, X., Xue, L., Ding, K., Liu, T., et al. (2023). Stratospheric aerosol and ozone responses to the Hunga Tonga-Hunga Ha'apai volcanic eruption. *Geophysical Research Letters*, *50*(4), e2022GL102315. https://doi.org/10.1029/2022gl102315

Manney, G. L., Santee, M. L., Lambert, A., Millán, L. F., Minschwaner, K., Werner, F., et al. (2023). Siege in the Southern Stratosphere: Hunga Tonga-Hunga Ha'apai water vapor excluded from the 2022 Antarctic polar vortex. *Geophysical Research Letters*, *50*(14), e2023GL103855. https://doi.org/10.1029/2023GL103855

Millan, L., Santee, M. L., Lambert, A., Livesey, N. J., Werner, F., Schwartz, M. J., et al. (2022). The Hunga Tonga-Hunga Ha'apai hydration of the stratosphere.

Quaglia, I., Timmreck, C., Niemeier, U., Visioni, D., Pitari, G., Brodowsky, C., et al. (2023). Interactive stratospheric aerosol models' response to different amounts and altitudes of SO 2 injection during the 1991 Pinatubo eruption. *Atmospheric Chemistry and Physics*, *23*(2), 921–948. https://doi.org/10.5194/acp-23-921-2023

Randel, W. J., Johnston, B. R., Braun, J. J., Sokolovskiy, S., Vömel, H., Podglajen, A., & Legras, B. (2023). Stratospheric water vapor from the Hunga Tonga–Hunga Ha'apai volcanic eruption deduced from COSMIC-2 radio occultation. *Remote Sensing*, *15*(8), 2167. https://doi.org/10.3390/rs15082167

Randel, W. J., & Newman, P. A. (1998). The stratosphere in the Southern Hemisphere. In *Meteorology of the Southern Hemisphere* (pp. 243–282). Springer.

Randel, W. J., Wu, F., Swinbank, R., Nash, J., & O'Neill, A. (1999). Global QBO circulation derived from UKMO stratospheric analyses. *Journal of the Atmospheric Sciences*, *56*(4), 457–474. https://doi.org/10.1175/1520-0469(1999)056<0457:gqcdfu>2.0.co;2

Richter, J. H., Glanville, A. A., Edwards, J., Kauffman, B., Davis, N. A., Jaye, A., et al. (2022). Subseasonal Earth system prediction with CESM2. *Weather and Forecasting*, *37*(6), 797–815. https://doi.org/10.1175/waf-d-21-0163.1

Rieger, L. A., Randel, W. J., Bourassa, A. E., & Solomon, S. (2021). Stratospheric temperature and ozone anomalies associated with the 2020 Australian New Year fires. *Geophysical Research Letters*, *48*(24), e2021GL095898. https://doi.org/10.1029/2021gl095898

Santee, M. L., Lambert, A., Froidevaux, L., Manney, G. L., Schwartz, M. J., Millán, L. F., et al. (2023). Strong evidence of heterogeneous processing on stratospheric sulfate aerosol in the extrapolar Southern Hemisphere following the 2022 Hunga Tonga-Hunga Ha'apai eruption. *Journal of Geophysical Research: Atmospheres*, *128*(16), e2023JD039169. https://doi.org/10.1029/2023JD039169

Santee, M. L., Lambert, A., Manney, G. L., Livesey, N. J., Froidevaux, L., Neu, J. L., et al. (2022). Prolonged and pervasive perturbations in the composition of the Southern Hemisphere midlatitude lower stratosphere from the Australian New Year's fires. *Geophysical Research Letters*, *49*(4), e2021GL096270. https://doi.org/10.1029/2021gl096270

Schoeberl, M. R., Wang, Y., Ueyama, R., Taha, G., Jensen, E., & Yu, W. (2022). Analysis and impact of the Hunga Tonga-Hunga Ha'apai stratospheric water vapor plume. *Geophysical Research Letters*, *49*(20), e2022GL100248. https://doi.org/10.1029/2022GL100248

Schoeberl, M. R., Wang, Y., Ueyama, R., Taha, G., & Yu, W. (2023). The cross equatorial transport of the Hunga Tonga-Hunga Ha'apai eruption plume. *Geophysical Research Letters*, *50*(4), e2022GL102443. https://doi.org/10.1029/2022GL102443

Sellitto, P., Podglajen, A., Belhadji, R., Boichu, M., Carboni, E., Cuesta, J., et al. (2022). The unexpected radiative impact of the Hunga Tonga eruption of 15th January 2022. *Communications Earth & Environment*, *3*(1), 288. https://doi.org/10.1038/s43247-022-00618-z

Solomon, S. (1999). Stratospheric ozone depletion: A review of concepts and history. *Reviews of Geophysics*, *37*(3), 275–316. https://doi.org/10.1029/1999rg900008

Solomon, S., Dube, K., Stone, K., Yu, P., Kinnison, D., Toon, O. B., et al. (2022). On the stratospheric chemistry of midlatitude wildfire smoke. *Proceedings of the National Academy of Sciences*, *119*(10), e2117325119. https://doi.org/10.1073/pnas.2117325119

Solomon, S., Garcia, R. R., Sherwood Rowland, F., & Wuebbles, D. J. (1986). On the depletion of Antarctic ozone. *Nature*, *321*(6072), 755–758. https://doi.org/10.1038/321755a0

Solomon, S., J Ivy, D., Kinnison, D., Mills, M. J., Neely, R. R., III, & Schmidt, A. (2016). Emergence of healing in the Antarctic ozone layer. *Science*, *353*(6296), 269–274. https://doi.org/10.1126/science.aae0061

Solomon, S., Rosenlof, K. H., Portmann, R. W., Daniel, J. S., Davis, S. M., Sanford, T. J., & Plattner, G.-K. (2010). Contributions of stratospheric water vapor to decadal changes in the rate of global warming. *Science*, *327*(5970), 1219–1223. https://doi.org/10.1126/science.1182488

Solomon, S., Stone, K., Yu, P., Murphy, D. M., Kinnison, D., Ravishankara, A. R., & Wang, P. (2023). Chlorine activation and enhanced ozone depletion induced by wildfire aerosol. *Nature*, *615*(7951), 259–264. https://doi.org/10.1038/s41586-022-05683-0

Stone, K. A., Solomon, S., Kinnison, D. E., Pitts, M. C., Poole, L. R., Mills, M. J., et al. (2017). Observing the impact of Calbuco volcanic aerosols on south polar ozone depletion in 2015. *Journal of Geophysical Research: Atmospheres*, *122*(21), 11–862. https://doi.org/10.1002/2017jd026987

Strahan, S. E., Smale, D., Solomon, S., Taha, G., Damon, M. R., Steenrod, S. D., et al. (2022). Unexpected repartitioning of stratospheric inorganic chlorine after the 2020 Australian wildfires. *Geophysical Research Letters*, *49*(14), e2022GL098290. https://doi.org/10.1029/2022gl098290

Tie, X., & Brasseur, G. (1995). The response of stratospheric ozone to volcanic eruptions: Sensitivity to atmospheric chlorine loading. *Geophysical Research Letters*, *22*(22), 3035–3038. https://doi.org/10.1029/95gl03057

Tilmes, S., Richter, J. H., Mills, M. J., Kravitz, B., MacMartin, D. G., Vitt, F., et al. (2017). Sensitivity of aerosol distribution and climate response to stratospheric SO_2 injection locations. *Journal of Geophysical Research: Atmospheres*, *122*(23), 12–591. https://doi.org/10.1002/2017jd026888

Vömel, H., Evan, S., & Tully, M. (2022). Water vapor injection into the stratosphere by Hunga Tonga-Hunga Ha'apai. *Science*, *377*(6613), 1444–1447. https://doi.org/10.1126/science.abq2299

Waters, J. W., Froidevaux, L., Harwood, R. S., Jarnot, R. F., Pickett, H. M., Read, W. G., et al. (2006). The earth observing system microwave limb sounder (EOS MLS) on the Aura satellite. *IEEE Transactions on Geoscience and Remote Sensing*, *44*(5), 1075–1092. https://doi.org/10.1109/tgrs.2006.873771

Yook, S., Thompson, D. W. J., & Solomon, S. (2022). Climate impacts and potential drivers of the unprecedented Antarctic ozone holes of 2020 and 2021. *Geophysical Research Letters*, *49*(10), e2022GL098064. https://doi.org/10.1029/2022gl098064

Yu, W., Garcia, R., Jia, Y., Smith, A., Wang, X., Randel, W., et al. (2023). Mesospheric Temperature and circulation response to the Hunga Tonga-Hunga-Ha'apai volcanic eruption. *Journal of Geophysical Research: Atmospheres*, *128*(21), e2023JD039636. https://doi.org/10.1029/2023JD039636

Yulaeva, E., Holton, J. R., & Wallace, J. M. (1994). On the cause of the annual cycle in tropical lower-stratospheric temperatures. *Journal of the Atmospheric Sciences*, *51*(2), 169–174. https://doi.org/10.1175/1520-0469(1994)051<0169:otcota>2.0.co;2

Zhang, J., Kinnison, D. E., Zhu, Y., Wang, X., Tilmes, S., Dubé, K. R., & Randel, W. J. (2023). Chemistry contribution to stratospheric ozone depletion after the unprecedented water rich Hunga Tonga eruption. https://doi.org/10.22541/essoar.169149953.33177277/v1

Zhu, Y., Bardeen, C. G., Tilmes, S., Mills, M. J., Wang, X., Lynn Harvey, V., et al. (2022). Perturbations in stratospheric aerosol evolution due to the water-rich plume of the 2022 Hunga-Tonga eruption. *Communications Earth & Environment*, *3*(1), 1–7. https://doi.org/10.1038/s43247-022-00580-w

Zhu, Y., Toon, O. B., Douglas, K., Lynn Harvey, V., Mills, M. J., Bardeen, C. G., et al. (2018). Stratospheric aerosols, polar stratospheric clouds, and polar ozone depletion after the Mount Calbuco eruption in 2015. *Journal of Geophysical Research: Atmospheres*, *123*(21), 12–308. https://doi.org/10.1029/2018jd028974

Zhu, Y., Toon, O. B., Lambert, A., Kinnison, D. E., Bardeen, C., & Pitts, M. C. (2017). Development of a polar stratospheric cloud model within the community earth system model: Assessment of 2010 Antarctic winter. *Journal of Geophysical Research: Atmospheres*, *122*(19), 10–418. https://doi.org/10.1002/2017jd027003